CHEMICAL PHYSICS

Momentum-dependent sum-frequency vibrational spectroscopy of bonded interface layer at charged water interfaces

Yao Hsiao†, Ting-Han Chou†‡, Animesh Patra, Yu-Chieh Wen*

Interface-specific hydrogen (H)–bonding network of water directly controls the energy transfer and chemical reaction pathway at many charged aqueous interfaces, yet to characterize these bonded water layer structures remains a challenge. We now develop a sum-frequency spectroscopic scheme with varying photon momenta as an all-optic solution for retrieving the vibrational spectra of the bonded water layer and the ion diffuse layer and, hence, microscopic structural and charging information about an interface. Application of the method to a model surfactant-water interface reveals a hidden weakly donor H-bonded water species, suggesting an asymmetric hydration-shell structure of fully solvated surfactant headgroups. In another application to a zwitterionic phosphatidylcholine lipid monolayer–water interface, we find a highly polarized bonded water layer structure associating to the phosphatidylcholine headgroup, while the diffuse layer contribution is experimentally proven to be negligible. Our all-optic method offers an in situ microscopic probe of electrochemical and biological interfaces and the route toward future imaging and ultrafast dynamics studies.

INTRODUCTION

Charged water interfaces are responsible for many natural phenomena (*1*, *2*) and of great importance in the development of advanced catalysts and energy storage devices (*3*–*5*). Microscopic structures of these interfaces are in general under the influences of two effects: One is the interface-specific bonding interactions among water molecules, solvated ions, and the substrate adjacent to water effectively within a few monolayers of water away from the interface. This region is labeled as "the bonded interface layer (BIL)" (*6*). Another effect is the dc electric field, E_0, set up by interfacial charges and diffuse ions in a much extended region [so-called "diffuse layer (DL)"] (*5*). It has been recognized that the BIL structure controls the microscopic pathways and equilibrium of interfacial reactions and, therefore, dictates diverse chemical and biological processes (*1*–*5*, *7*–*10*). For example, the photoionization reaction of phenol proceeds 10^4 times faster at the water surface than in the bulk aqueous phase owing to distinct hydration environments (*9*). Water molecules at biomembranes assist the in-plane proton conductivity along the membrane, which is vital for cellular bioenergetics (*2*, *10*). Despite its importance, current knowledge on microscopic structure and the interplay between ionic and molecular species in the BIL is very limited due to paucity of nowadays experimental techniques (*8*, *11*–*13*). For example, scanning probe microscopies (*11*) and x-ray adsorption spectroscopy (*12*) cannot yield information on the geometry or strength of water H bonds, and infrared and Raman spectroscopies cannot distinguish the BIL from the DL (*13*).

Vibrational sum-frequency (SF) generation (SFG) dictated by symmetry has been developed as a versatile surface analytical tool for investigating the BIL at various (charge-neutral) aqueous surfaces (*9*, *14*). At charged water interfaces, however, the surface specificity of this method is largely degraded because the emergence of a dc field in the DL enables SFG from bulk water via the third-order optical nonlinearity, $\chi^{(3)}$ (*6*, *15*). Interference between the SF fields from BIL and DL not only hides vibrational signatures of the BIL (*6*, *16*) but also causes artificial resonances in the interfered spectra (*17*). Separating the two contributions appears crucial but remains challenging so far (*6*, *16*–*23*). In many reports, one of the two contributions was simply assumed constant or negligible (*18*–*20*). In others, the DL was intentionally screened by adding considerable (external) ions in solutions, but the consequent disturbances of the BIL structure and chemistry therein were hardly addressed (*21*, *22*). In 2016, Tian, Shen, and colleagues proposed an SFG scheme for retrieving the (intrinsic) BIL spectra, which required prior information about the surface charge density (*6*). The idea was first demonstrated using carboxylic-acid monolayer on water (*6*) and later realized by Gibbs group for the silica/water interface with help from the electrokinetic measurements (*16*). A different gate-control scheme was recently proposed by Wang *et al.* using an electrolyte-insulator-semiconductor field-effect transistor (FET) configuration (*23*). Despite the success in (*6*) and (*23*), the demonstrations relied on specific interfaces that allow spectroscopic quantification of all charged surface species or integration with a FET. While the combination of SFG and electrokinetic measurements is ideal for better applicability (*16*), comparing the two independent measurements would be difficult as knowing that the local surface structure could be easily influenced by surface preparations (*24*) and measurement conditions (*25*, *26*) and may vary sample by sample (*27*).

In this paper, we develop an all-optic scheme for direct and in situ determination of the vibrational spectra of BIL at various water interfaces. The scheme is realized by detecting a set of SF radiations from a sample with varying input photon momenta. This idea, first proposed in 2016 (*6*), was recently examined theoretically in a thorough manner (*28*). Here, we report experimental results supporting its validity and demonstrate its viability to different interfaces. Its

Institute of Physics, Academia Sinica, Taipei 11529, Taiwan, R. O. C.
†These authors contributed equally to this work.
‡Present address: Max Planck Institute for the Structure and Dynamics of Matter, 22761 Hamburg, Germany.
*Corresponding author. Email: ycwen@phys.sinica.edu.tw

application to zwitterionic phosphatidylcholine (PC) lipid/water interfaces shows a highly polarized bonded water layer structure associating to the PC headgroup, while the DL contribution to SFG is proven to be negligible. In another application to a model charged surfactant-water interface, the result reveals a hidden weakly donor H-bonded water species in the BIL, revealing the hydration structure of the surfactant headgroup. This technique offers a viable means for in situ probing of electrochemical and aqueous biological interfaces at the molecular level.

Theory

We follow (*6*) to formulate the SFG process at a charged water interface next to an isotropic medium with z along the surface normal. The reflected SFG from such an interface has its field proportional to the effective surface nonlinear susceptibility, $\chi^{(2)}_{S,eff}(\omega_{SF} = \omega_1 + \omega_2)$, which can be expressed as

$$\chi^{(2)}_{S,eff} = \chi^{(2)}_{BIL} + \int_{0^+}^{\infty} \chi^{(3)}(z') \cdot \hat{z} E_0(z') e^{i\Delta k_z z'} dz' = \chi^{(2)}_{BIL} + \chi^{(2)}_{DL}$$
$$\chi^{(2)}_{DL} \equiv \int_{0^+}^{\infty} \chi^{(3)}(z') \cdot \hat{z} E_0(z') e^{i\Delta k_z z'} dz' \cong \chi^{(3)}_B \cdot \hat{z} \Psi \quad (1)$$

with $\Psi \equiv \int_{0^+}^{\infty} E_0(z') e^{i\Delta k_z z'} dz'$

Here, $\chi^{(2)}_{BIL}$ and $\chi^{(2)}_{DL}$ denote the nonlinear optical susceptibilities of the BIL (at $z = 0^-$ to 0^+) and DL, respectively. $\Delta k_z = k_{SF,z} + k_{1,z} + k_{2,z}$ describes the phase mismatch for reflected SFG (*29*, *30*). We have considered that (i) the DL (approximately, at $z > 0^+$) is characterized by the third-order nonlinear susceptibility of bulk water, $\chi^{(3)}_B$, (*31*) with negligible electric-quadrupole contribution (*30*), and (ii) $|\chi^{(2)}_{BIL}| \gg |\int_{0^-}^{0^+} \chi^{(3)}(z') \cdot \hat{z} E_0(z') dz'|$ in the BIL due to stronger influences of the H bonding compared to the mean-field–induced electrostatic energy (*16*).

To separate $\chi^{(2)}_{BIL}$ and $\chi^{(2)}_{DL}$ in Eq. (1), we compare two measurements with different Δk_z (labeled below for all symbols with a superscript *A* or *B*), which are related through Eq. (1) by

$$\chi^{(2),B}_{S,eff} = \chi^{(2),A}_{S,eff} + \Delta\chi^{(2)}_{DL}$$
$$\Delta\chi^{(2)}_{DL} \equiv \chi^{(2),B}_{DL} - \chi^{(2),A}_{DL} = \chi^{(3)}_B \cdot \hat{z} \int_{0^+}^{\infty} E_0(z') \left(e^{i\Delta k_z^B z'} - e^{i\Delta k_z^A z'}\right) dz' \quad (2)$$

It is clear that $\Delta\chi^{(2)}_{DL}$ senses $E_0(z)$ with a weighting factor $(e^{i\Delta k_z^B z} - e^{i\Delta k_z^A z})$ that approaches to zero as $z \ll \Delta k_z^{-1}$ (= coherence length l_c). It indicates that $\Delta\chi^{(2)}_{DL}$ cannot be sensitive to subtle ionic packing structure and potential profile at the immediate neighborhood of the interface, as described by various electric double layer (EDL) models (*5*, *32*), but reflects essentially the Poisson-Boltzmann (PB) ion distribution on the length scale of l_c (about tens of nanometers), i.e., the diffuse layer. Therefore, $\Delta\chi^{(2)}_{DL}$ represents a differential contribution from the DL detected with two effective probing depths (l_c^A versus l_c^B, as sketched in Fig. 1A). It offers a probe to the potential drop across the DL (so-called "diffuse layer potential", ϕ_0), with $\phi_0 \cong \int_{0^+}^{\infty} E_0(z) dz$.

Without the loss of validity, we propose to measure complex $\chi^{(2),A}_{S,eff}$ and intensity $|\chi^{(2),B}_{S,eff}|^2$ spectra for a given sample. With the previously measured $\chi^{(3)}_B(\omega_2)$ of bulk water (*6*), we can use Eq. 2 to fit the measured $|\chi^{(2),B}_{S,eff}(\omega_2)|^2$ spectrum with the complex $\chi^{(2),A}_{S,eff}(\omega_2)$ through the PB theory (*5*, *15*) that relates $E_0(z)$ to ϕ_0 and the ionic strength. Having the only fitting variable ϕ_0 deduced, we then follow (*6*) to estimate $\chi^{(2),A}_{DL}(\omega_2)$ from Eq. 1 with the known $\chi^{(3)}_B(\omega_2)$ and the PB theory and subsequently determine the complex $\chi^{(2)}_{BIL}(\omega_2)$ spectrum from the difference between the measured $\chi^{(2),A}_{S,eff}(\omega_2)$ and the estimated $\chi^{(2),A}_{DL}(\omega_2)$. Note that the retrieved $\chi^{(2)}_{BIL}(\omega_2)$ is independent of the EDL models in terms of the non-PB–distributed interfacial ionic structure assumed.

This proposed method is labeled below as "momentum-dependent SF vibrational spectroscopy (MD-SFVS)". This scheme with varying Δk_z is conceptually similar to the earlier experiments by Shen and colleagues (*29*, *30*) and by Hore and Tyrode (*33*). The former was designed for resolving bulk quadrupolar contributions to SF spectra (*29*, *30*). In the latter, the authors evaluated the BIL and DL contributions to the integrated SF intensity versus Δk_z without spectral information (*33*). In our work, the additional phase measurement allows direct retrieval of the BIL and DL spectra.

RESULTS

Spectral decomposition by MD-SFVS experiment

Our MD-SFVS measurements with l_c^A of 45 nm and l_c^B of 66 to 73 nm were performed in situ with a modified phase-sensitive SFVS setup with S, S, and P (SSP)–polarized SF, near-infrared (NIR), and mid-infrared (MIR) fields. As sketched in Fig. 1A, the setup comprises two SFG configurations for different Δk_z. They share the same femtosecond MIR input with an angle of incidence of 45° but have separate narrow-band NIR input pulses with distinct wavelengths λ and angles of incidence θ. (For l_c^A, λ = 0.8 μm and θ = 45°; for l_c^B, λ = 1.2 to 1.4 μm and θ = 64°; see Materials and Methods for details). The measured spectra of a sample were normalized against a z-cut quartz reference and shown below in meter-kilogram-second (MKS) units after correcting the Fresnel coefficients. High spectroscopic specificity to $\Delta\chi^{(2)}_{DL}$ is first confirmed by inspecting the OH stretch SF intensity spectra of the neat water/air interface versus a charged surfactant [cetyltrimethylammonium bromide (CTAB)]/water interface (see Materials and Methods for sample preparation). As shown in Fig. 1B, the measured spectra of the neat water surface are essentially the same upon changes in Δk_z, as expected for a charge-neutral interface with $\chi^{(2),A}_{S,eff} = \chi^{(2),B}_{S,eff} = \chi^{(2)}_{BIL}$. (See fig. S3 for raw data without Fresnel correction). By contrast, the charged CTAB/water interface shows a manifest correlation between Δk_z and the SFG strength (Fig. 1C), i.e., the strength increases by ~40% with a notable change in l_c from 45 to 66 nm and increases by 4 to 9% with a minor change in l_c from 66 to 73 nm. It is such a difference disclosing the emergence of a DL ($\chi^{(2),B}_{S,eff} = \chi^{(2),A}_{S,eff} + \Delta\chi^{(2)}_{DL}$) and being the basis for the spectral separation.

More quantitatively, we adopted a closely packed lignoceric acid (LA) ($C_{23}H_{47}COOH$) monolayer on water to verify the spectral separation by MD-SFVS. Deprotonation of this monolayer (COOH ↔

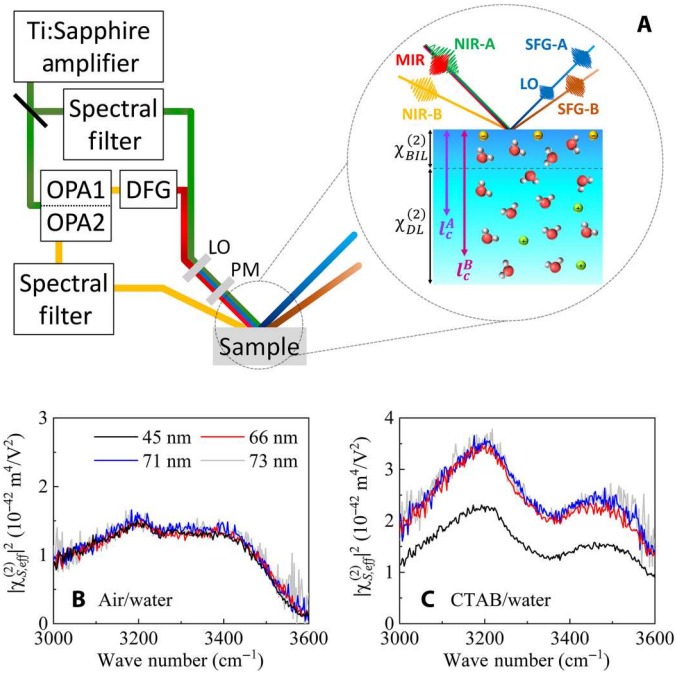

Fig. 1. MD-SFVS of charged water interfaces. (**A**) Illustration of the MD-SFVS setup and a charged interfacial structure probed. The SF field, SFG-A (SFG-B), was emitted through mixing of an MIR pulse with one of the two NIR fields, NIR-A (NIR-B), and detected through the heterodyne (homodyne) scheme with a coherence length of l_c^A (l_c^B). LO and PM refer to local oscillator and phase modulator, respectively. The optical inputs were prepared by a Ti:sapphire amplifier equipped with two optical parametric amplifiers (OPAs), difference-frequency generation (DFG), and two grating-based spectral filters. See Materials and Methods for details. (**B** and **C**) $|\chi^{(2)}_{S,eff}|^2$ SF intensity spectra of the surfaces of (B) neat water and (C) a 10 μM CTAB solution measured by MD-SFVS with different coherent lengths.

$COO^- + H^+$) with subphase pH and the resultant spectral changes have been well studied by SFVS (*6*, *34*); it was shown that the interface is charge-neutral at low pH (<~2) but increasingly negatively charged with pH upon deprotonation of the monolayer. Knowing that the fractional ionization of this monolayer is less than few percent at acidic pH (2 to 7) (*6*), the induced structural perturbation on the BIL is hardly detected. Therefore, we anticipate that $\chi^{(2)}_{BIL}(\omega_2)$ retrieved from MD-SFVS in this pH region is invariant and similar to $\chi^{(2)}_{S,eff}(\omega_2) \cong \chi^{(2)}_{BIL}(\omega_2)$ at pH < 2 and also expect the deduced ϕ_0 versus pH to follow the acid dissociation constant pK_a. Figure 2A shows the SF intensity spectra of the samples measured at three acidic pH in the OH-stretching region. They are very similar to the earlier report (*6*), but the effect of varying Δk_z is presented here for the first time. It is seen that the nearly charge-neutral interface at pH 2.1, again, exhibits Δk_z-insensitive SF spectra, whereas the SF intensity at pH 4.1 and 5.7 varies prominently with Δk_z, revealing appearance of the DL due to the monolayer ionization.

We follow the two-step analysis described above to decompose the spectra. First, we use the measured $\chi^{(2),A}_{S,eff}(\omega_2)$ and the known $\chi^{(3)}_B(\omega_2)$ (*6*) to fit the measured $|\chi^{(2),B}_{S,eff}(\omega_2)|^2$ spectra via Eq. 2 with the PB theory (*5*) for deducing ϕ_0. Second, we use Eq. 1 to estimate $\chi^{(2),A}_{DL}(\omega_2)$ from ϕ_0 with the known $\chi^{(3)}_B(\omega_2)$ and the PB theory and then obtain $\chi^{(2)}_{BIL}(\omega_2)$ from the difference between the measured $\chi^{(2),A}_{S,eff}(\omega_2)$ and the estimated $\chi^{(2),A}_{DL}(\omega_2)$. As seen in Fig. 2A, the fitting quality for the $|\chi^{(2),B}_{S,eff}|^2$ spectra of the two charged interfaces is reasonably well. (See fig. S4 for fits with different values of ϕ_0.) The diffuse layer potential so obtained indicates that the interface is negatively charged with $\phi_0 = -70 \pm 7$ mV at pH 4.1 and $\phi_0 = -191 \pm 11$ mV at pH 5.7. One could compare these estimates with the calculation via the deprotonation reaction equation for fatty acids with pK_a of 5.1 to 5.6 (*6*, *34*), which yields $\phi_0 = -77 \pm 10$ mV at pH 4.1 and $\phi_0 = -170 \pm 10$ mV at pH 5.7 and indeed find the agreement. [See (*6*) for the detailed calculation.] Furthermore, even with the appreciable pH dependency of ϕ_0 and the measured spectra (Fig. 2A), the complex $\chi^{(2)}_{BIL}$ vibrational spectra retrieved at pH 4.1 and 5.7 (Fig. 2, B and C) are found consistent with $\chi^{(2)}_{BIL}$ ($\cong \chi^{(2),A}_{S,eff}$) at pH 2.1, as expected for a RCOOH–dictated interfacial H-bonding structure with trivial perturbations by sparse $RCOO^-$.

Charge neutrality of zwitterionic PC lipid/water interfaces

With the validity of the spectral separation confirmed, one can now apply the scheme to various aqueous interfaces without assumption or prior information about the interface. We offer two demonstrations and show that, even in well-investigated cases, the results could provide additional information owing to the spectral separation. We first examine charge neutrality of the zwitterionic PC lipid monolayer/water interface as a quick qualitative application of MD-SFVS. Such an interface is known to have great biological relevance because of the key role of PC lipids in constituting the membranes. In many SFVS studies, the spectrum interpretation relied on the nominal charge neutrality of the zwitterionic headgroup (*35*, *36*). However, the zeta potential for liposomes of PC lipids has been reported to be negative at pH 7 (*37*). It was also argued that the PC monolayers on neat water were positively charged due to partial deprotonation of the phosphate groups with pK_a in the range of 1 to 3 (*38*). Whether it is valid to presume negligible $\chi^{(2)}_{DL}(\omega_2)$ in interpreting the SF spectra appears to be questionable.

We resolve this problem simply by MD-SFVS. To examine the intrinsic effects of the PC headgroup, the studied samples include two types of PC monolayers on water: 1,2-dipalmitoyl-*sn*-glycero-3-phosphocholine (DPPC) Langmuir monolayer and hexadecyl phosphocholine (HePC) Gibbs monolayer (see Materials and Methods for the sample preparation). HePC has the same headgroup but differs from DPPC in terms of its single alkyl chain and lack of the glycerol backbone. Figure 3 shows the measured SF intensity spectra for the two types of monolayers on water at bulk pH ~7. Both interfaces are seen to display very intense OH-stretching resonances with strengths, e.g., 3.4×10^{-41} m^4/V^2 for HePC, readily comparable to these from many charged aqueous interfaces with substantial $\chi^{(3)}_B$ contributions (See fig. S1 for examples). Using MD-SFVS, we find that these spectra of the PC–water interfaces are invariant upon the change in Δk_z, evidencing their charge neutrality and ignorable $\chi^{(2)}_{DL}(\omega_2)$. With the molecular origin clarified, one can now safely attribute the observed strong SF resonance solely to a highly polarized bonded water layer structure associating to the PC headgroup. This is likely due to the local dipolar field generated between the charged phosphate and choline and/or a H-

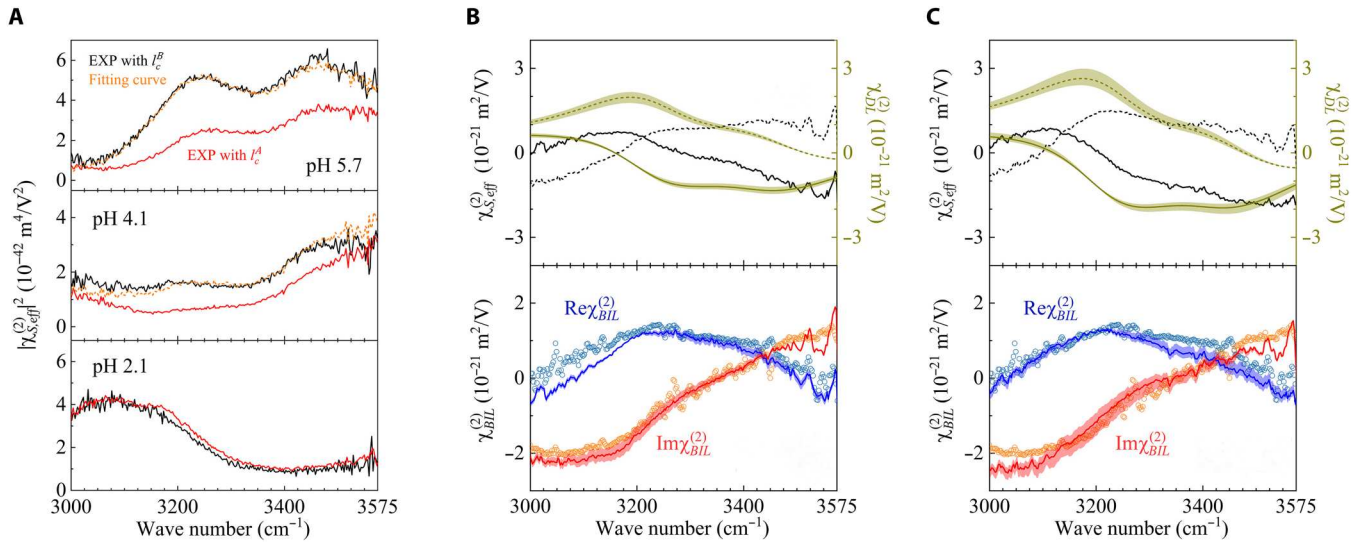

Fig. 2. Analysis of the MD-SFVS results of the LA monolayer/water interface. (**A**) $|\chi^{(2)}_{S,eff}|^2$ SF intensity spectra at pH 2.1, 4.1, and 5.7 measured with the coherence lengths of l_c^A and l_c^B (solid lines). Dashed lines denote the fits for $|\chi^{(2),B}_{S,eff}(\omega_2)|^2$ based on complex $\chi^{(2),A}_{S,eff}(\omega_2)$ from (B) and (C). (**B** and **C**) Measured $\chi^{(2),A}_{S,eff}(\omega_2)$ and the retrieved $\chi^{(2),A}_{DL}(\omega_2)$ and $\chi^{(2)}_{BIL}(\omega_2)$ spectra at (B) pH 4.1 and (C) pH 5.7 (lines). Top: Solid (dashed) lines denote real (imaginary) part of $\chi^{(2),A}_{S,eff}(\omega_2)$ and $\chi^{(2),A}_{DL}(\omega_2)$. Bottom: The complex $\chi^{(2)}_{BIL}(\omega_2)$ retrieved at pH 4.1 or 5.7 (lines) is compared with $\chi^{(2)}_{BIL}(\omega_2)$ [$\cong \chi^{(2)}_{S,eff}(\omega_2)$] measured at pH 2.1 (dots). The shadowed regions in (B) and (C) denote uncertainties. Consistency of the retrieved $\chi^{(2)}_{BIL}(\omega_2)$ at the three acidic pH confirms validity of the MD-SFVS analysis.

bonding structure of water bridging both phosphate and choline, as proposed by Morita and colleagues (*39*) and Bonn and colleagues (*8*, *36*). A brief discussion about the BIL structure via the $\mathrm{Im}\chi^{(2)}_{BIL}$ ($\cong \mathrm{Im}\chi^{(2)}_{S,eff}$) spectra is given in note S1.

BIL structure of surfactant/water interfaces

Strengths of MD-SFVS are further demonstrated using charged surfactant/water interfaces, for which we focus on the microscopic hydration structure of the adsorbed surfactants. This fundamental issue remains poorly understood and is a subject of hot debate (*17*, *40*, *41*). It is addressed below through the newly deduced $\mathrm{Im}\chi^{(2)}_{BIL}(\omega_2)$. [Note that it cannot be retrieved using zeta potential (*16*) that characterizes a dynamic system in the electrokinetic measurement where the surfactant may never reach adsorption equilibrium (*26*).]

We performed MD-SFVS measurements on the air/water interface with a series of CTAB concentrations in water and analyzed the results via the two-step analysis described above to deduce ϕ_0, $\chi^{(2),A}_{DL}(\omega_2)$, and $\chi^{(2)}_{BIL}(\omega_2)$ in order. Shown in Figs. 4 and 5A are the measured $|\chi^{(2)}_{S,eff}|^2$ and $\mathrm{Im}\chi^{(2)}_{S,eff}$ OH-stretching spectra, respectively, which are essentially similar to those reported earlier for given CTAB concentrations (*42*) (less than 3% of the critical micelle concentration). From Fig. 4, the difference of the SF intensity for $\Delta k_z = \Delta k_z^A$ versus Δk_z^B increases with the bulk CTAB concentration, reflecting increasing $|\Delta\chi^{(2)}_{DL}|$ and surface charges due to CTA^+ adsorption. We can, again, fit the $|\chi^{(2),B}_{S,eff}(\omega_2)|^2$ spectra reasonably well with the measured $\chi^{(2),A}_{S,eff}(\omega_2)$ and the known $\chi^{(3)}_B(\omega_2)$ (*6*), yielding increasingly positive-valued ϕ_0. (See figs. S4B and S5 for the deduced ϕ_0 and details of the fitting.) As for $\mathrm{Im}\chi^{(2),A}_{S,eff}(\omega_2)$ in Fig. 5A, it exhibits an obvious bipolar spectral distortion with respect to the neat water surface upon surface adsorption of CTAB. By decomposing it into $\mathrm{Im}\chi^{(2),A}_{DL}(\omega_2)$ and $\mathrm{Im}\chi^{(2)}_{BIL}(\omega_2)$ with the deduced ϕ_0, we verify that the observed change of $\mathrm{Im}\chi^{(2),A}_{S,eff}(\omega_2)$ comes mainly from the emergent $\mathrm{Im}\chi^{(2),A}_{DL}(\omega_2)$ (Fig. 5B), and the bipolar spectral shape of $\mathrm{Im}\chi^{(2),A}_{DL}(\omega_2)$ does not reveal real vibrational signatures but a consequence of absorptive-dispersive mixing of $\chi^{(3)}_B(\omega_2)$ via complex Ψ through Eq. 1 (*17*). For example, a positive hump in $\mathrm{Im}\chi^{(2),A}_{DL}(\omega_2)$ at ~3600 cm^{-1} appears as an artificial resonance owing to the contribution from $\mathrm{Re}\chi^{(3)}_B(\omega_2)$, which was known to arise recent debates (*17*, *43*, *44*).

With $\mathrm{Im}\chi^{(2),A}_{DL}(\omega_2)$ removed from $\mathrm{Im}\chi^{(2),A}_{S,eff}(\omega_2)$, unambiguous vibrational signatures of the interface can be identified through the $\mathrm{Im}\chi^{(2)}_{BIL}(\omega_2)$ spectra (Fig. 5C). They look similar to the neat water surface but display modified resonances above 3400 cm^{-1} for [CTAB] ≥ 10 μM, disclosing surfactant-induced structural perturbation on the BIL. This spectral modification comprises an emergent positive band at ~3610 cm^{-1} with a linewidth of ~240 cm^{-1} and relatively small changes of the free OH resonance (that red shifts by 4 ± 2 cm^{-1} with its amplitude reduced by 16 ± 6% for [CTAB] = 30 μM), as revealed by spectrum analyses based on approximation of discrete Lorentzian resonances. (See note S2 for details).

The emergent positive 3610-cm^{-1} band must result from OH stretching of weakly donor-bonded water molecules of varying strengths and geometries with a net upward O → H orientation (toward air). In interpreting their origin, one may consider water molecules associating to hydrophobic tail or headgroup of the surface CTAB. The former is likely irresponsible because the involved van der Waals interaction is usually too weak to cause an

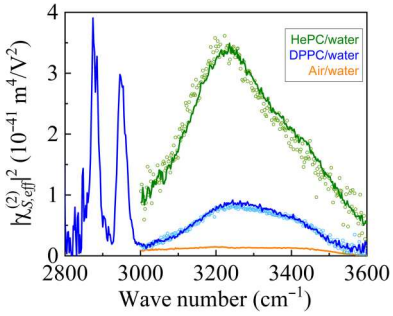

Fig. 3. SF intensity spectra of zwitterionic PC lipid monolayer–water interface. Spectra for a closely packed DPPC Langmuir monolayer/water interface and the HePC Gibbs monolayer on a 1.6 μM HePC solution with subphase pH of 7.0 and 7.8, respectively, are shown in comparison with the neat water/air interface in the OH-stretching region. Lines and dots denote the results measured with $l_c = l_c^A$ and l_c^B, respectively, and their consistency indicates a negligible DL and the responsible role of the BIL in SFG. CH-stretching vibrations of the DPPC molecules reveal nearly vertical alignment of the alkyl chains and negligible gauche defects in the monolayer.

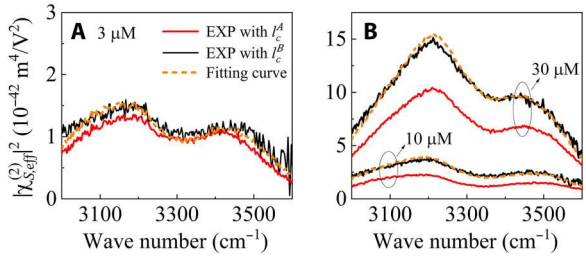

Fig. 4. SF intensity spectra of the surfaces of CTAB solutions. (**A**) 3 μM and (**B**) 10 and 30 μM bulk CTAB concentrations in the solutions. Solid lines denote $|\chi^{(2)}_{S,eff}(\omega_2)|^2$ measured with $l_c = l_c^A$ and l_c^B, and dashed lines denote the fits for $|\chi^{(2),B}_{S,eff}(\omega_2)|^2$ based on the measured complex $\chi^{(2),A}_{S,eff}(\omega_2)$ from Fig. 5A.

obvious spectral change more than perturbation of the dangling OH frequency (*19*). As for the latter, we explain the 3610-cm^{-1} band by considering an asymmetric hydration-shell structure of a fully solvated surfactant headgroup at the interface. This can be seen as follows. If the CTA^+ is partially desolvated at the water surface, the broken up-down symmetry of its hydration shell causes more H–down-oriented water molecules with O facing the CTA^+. This configuration cannot explain our observation due to inconsistent net polar orientation of the associated water molecules. On the other hand, as the CTA^+ is fully solvated, the hydration water molecules have comparable probabilities in orientations having dipoles pointing up and down, but they are influenced by an asymmetric interfacial environment. The bottom part of the hydration shell must comprise more water molecules with downward-pointing OHs donor H-bonded to their water neighbors, whereas the upper counterpart of the shell is likely to include more H–up-oriented water molecules exposing to air (or the alkyl chain) and thus rarely (or weakly) donor H-bonded, as sketched in Fig. 6. The distinct bonding conditions cause a relative frequency shift so that their spectral contributions cannot fully compensate each other. The high-frequency residual, dominated by the weakly donor-bonded H–up-oriented water molecules in the upper part of the shell, explains the 3610-cm^{-1} band.

For more details, the moderate red shift of the 3610-cm^{-1} band with respect to the free OH peak can be understood by considering association of the water molecules to the CTA^+ through water oxygen (*45*). Water molecules with various extents of the association would account for the highly broadened linewidth of this band. Our spectral assignment to this water species is supported by the observation that the free OH resonance weakens in the same CTAB concentration range where the 3610-cm^{-1} band emerges (see note S2 for details). This correlation suggests that both spectral signatures originate from a distorted local structure at the outmost water molecular layer in terms of annihilation of unperturbed free OH groups and creation of hydration water molecules surrounding the CTA^+. Through the analysis with discrete resonance approximation, we further deduce a lower-bound estimate of the surface density of water molecules contributing to the 3610-cm^{-1} band, suggesting >13 outmost-layer water molecules affected per single adsorbed CTAB (see note S2 for details). The scenario derived here is in line with a recent observation on reorientation of free-OH water molecules through the water bending mode (*41*).

Besides the first hydration shell of CTA^+, we have taken other headgroup–water bonding configurations into account but failed to find another feasible explanation for the 3610-cm^{-1} band. First, one may consider a symmetry-broken hydration shell of the Br^- ion. Possible association of Br^- to the surface CTA^+ breaks the up-down symmetry of the hydration shell, resulting in more H–up-oriented water molecules surrounding the Br^-. However, the binding interaction of water to the anion was known to cause much lower OH stretch frequencies compared to our observation, as shown, for example, by Smith *et al.* (*13*) in a Raman study. Another possibility is water molecules in the second hydration shell surrounding CTA^+ with their net upward OH(s) weakly donor bonded to the electron-deficient oxygen of water molecules in the first hydration shell, as proposed by Patra *et al.* (*46*) in explaining the effect of metallic ions on bulk water spectra. This scenario relies on strong binding (electron transfer) between the first-shell water molecules and the cation and is, therefore, unlikely in our case due to much weaker binding interactions with the large CTA^+ group [5.1 Å in radius (*47*)].

Sensitivity and analysis errors of MD-SFVS

The sensitivity and analysis errors of the MD-SFVS scheme depend on $e\phi_0/k_BT$ with e the elementary charge, k_B the Boltzmann constant, and T the temperature. For $e\phi_0/k_BT \ll 1$, one can adopt the Debye-Hückle approximation to simplify Eqs. 1 and 2, yielding

$$\Delta\chi^{(2)}_{DL} = (\chi^{(3)}_B \cdot \phi_0) \cdot [(1 - i\lambda_D \Delta k_z^B)^{-1} - (1 - i\lambda_D \Delta k_z^A)^{-1}]$$
$$\chi^{(2),A}_{DL} = (\chi^{(3)}_B \cdot \phi_0) \cdot (1 - i\lambda_D \Delta k_z^A)^{-1} \quad (3)$$

with λ_D as the Debye screening length. As expected, one should adopt a large variation of Δk_z and avoid the condition $\lambda_D \Delta k_z^A$, $\lambda_D \Delta k_z^B \ll 1$ for optimizing the sensitivity of the probed $\Delta\chi^{(2)}_{DL}$ to ϕ_0. (Note that λ_D varies with respect to electrolyte concentration and pH.) In addition, Eq. 3 shows the analysis error arising from the measurement uncertainty of the reported $\chi^{(3)}_B(\omega_2)$ spectrum (*6*). This uncertainty propagates into the deduced ϕ_0 but is effectively balanced and thus causes much moderate influences on the retrieved $\chi^{(2),A}_{DL}$ and $\chi^{(2)}_{BIL}$. For an intuition, one can notice from Eq. 3

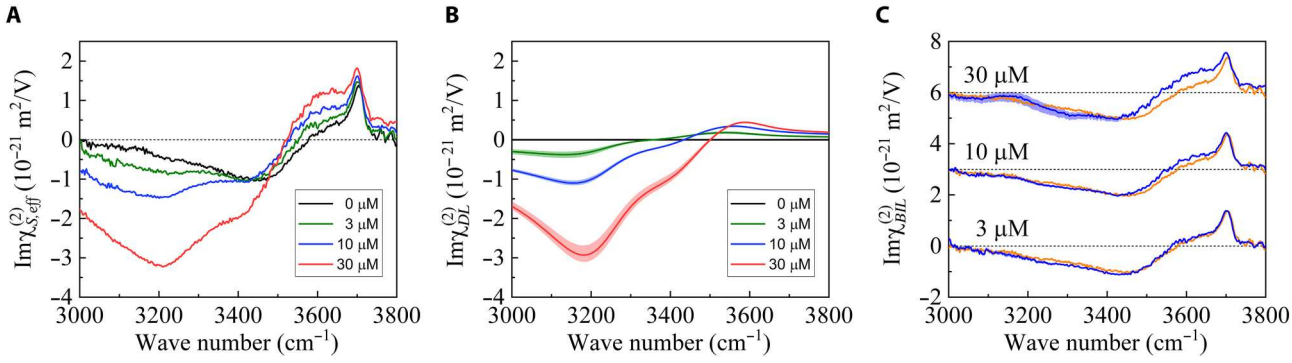

Fig. 5. Analysis of the MD-SFVS results of the air/water interface with different CTAB concentrations in water. (**A**) Measured Im$\chi^{(2),A}_{S,eff}$ spectra and (**B**) the retrieved Im$\chi^{(2),A}_{DL}$ spectra (solid lines). (**C**) Im$\chi^{(2)}_{BIL}$ spectra retrieved from (A) and (B) (blue lines), in comparison with that of the neat water surface (orange lines). The data are vertically shifted for clarity. The shadowed regions in (B) and (C) denote uncertainties, and the dashed lines in (A) and (C) depict zero.

that a percentage error of $\chi^{(3)}_B$ is directly transferred to ϕ_0 via the experimentally observed $\Delta\chi^{(2)}_{DL}$ in an inverse manner, such that the errors of $\chi^{(3)}_B$ and ϕ_0 counteract each other in deducing $\chi^{(2),A}_{DL}$ and $\chi^{(2)}_{BIL}$. As for $e\phi_0/k_BT \gg 1$, the spatial distributions of diffuse ions and $E_0(z)$ are known to shrink in depth by following nonlinear PB equations. It causes that $\Delta\chi^{(2)}_{DL}$ is no longer proportional to ϕ_0 but exhibits a sublinear dependence on ϕ_0 and, hence, induces appreciable analysis errors in deducing ϕ_0 and $\chi^{(2)}_{BIL}$ through $\Delta\chi^{(2)}_{DL}$ for high ϕ_0 (typically >0.2 V). [See figs. S6 and S7 and (*48*) for detailed discussions.]

DISCUSSION

In summary, we have developed an SFVS scheme with varying photon momenta to directly probe vibrational spectra of the BIL at charged water interfaces. The method does not rely on prior information about the interfaces or assumption of the EDL models and is viable to aqueous interfaces next to any molecular/substrate system. Application of the method to the zwitterionic PC lipid monolayers on water revealed a highly polarized bonded water layer structure associating to the PC headgroup, while the DL contribution was experimentally proven to be negligible. In another application to the model surfactant (CTAB)/water interface, our result showed a hidden weakly donor H-bonded water species in the BIL, unveiling an asymmetric hydration structure of the surfactant headgroup. Our all-optic method offers an in situ microscopic probe of electrochemical and biological interfaces and the route toward future imaging and ultrafast dynamics studies. Moreover, this work highlights the opportunities of applying momentum-resolved nonlinear optics to explore surface excitations in bulk backgrounds, which generally include odd-order nonlinearities and even-order electric quadrupoles and electric dipoles (for crystals without inversion symmetry). What we develop here therefore broadens the application of surface nonlinear optics to general condensed matter research.

MATERIALS AND METHODS

Sample preparation

LA (>99% purity), CTAB (>99%), HePC (>99%), HCl (37 weight % water solution, reagent grade), NaOH (reagent grade, pellets), and chloroform (anhydrous grade, stabilized with ethanol) were obtained from Sigma-Aldrich. DPPC was purchased as lyophilized powders from Avanti Polar Lipids. All chemicals were used as received. Water was deionized by a Millipore system and had a resistivity of 18.2 megohm-cm. Its pH was varied by solvation of NaOH and HCl.

We follow (*6*) and (*48*) to prepare Langmuir monolayers on water in a thoroughly cleaned Teflon Langmuir trough. LA or DPPC was spread from a chloroform solution onto the aqueous surface, and the solvent was then allowed to evaporate for ~10 min. The monolayer of LA or DPPC was then compressed to the surface pressure of ~27 mN/m, corresponding to a closely packed monolayer in the tilted condensed phase. The CTAB and HePC monolayers on water were formed by following the Gibbs adsorption kinetics with a surface coverage controlled by the bulk concentration.

MD-SFG spectroscopy

Our MD-SFVS setup was based on a modified phase-sensitive SFVS with three fundamental inputs prepared by a 1-kHz, 50-fs Ti:sapphire laser system (Astrella, Coherent) equipped with two optical parametric amplifiers (OPAs) and two grating-based spectral filters (GSFs). In particular, (i) the femtosecond MIR input pulse with a bandwidth of ~250 cm^{-1} was generated from one OPA pumped by the Ti:sapphire laser, followed by difference-frequency generation using $AgGaS_2$. (ii) One narrowband fundamental input for SFVS with l^A_c (labeled as "the NIR-A pulse") was generated from the Ti:sapphire output at ~800 nm, with its bandwidth reduced to be ~13.6 cm^{-1} by a GSF. (iii) Another narrowband input for SFVS with l^B_c (labeled as "the NIR-B pulse") came from the signal output of the second OPA with a tunable wavelength λ. Its bandwidth reduced by another GSF was ~30 cm^{-1}, which was appropriate to characterize the H-bonded OH-stretching continuum without noticeable spectrum smoothing.

In phase-sensitive SFVS measurements with l^A_c configuration, the MIR and NIR-A pulses were focused onto the sample surface with the angle of incidence of 45° after copropagating through a

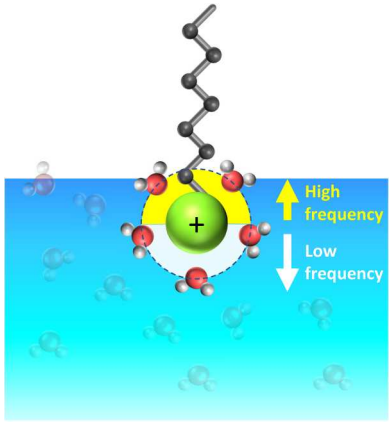

Fig. 6. Schematic representation of the asymmetric hydration-shell structure of a fully solvated surfactant headgroup. The up-down asymmetry of the hydration shell induced by a surface-specific bonding environment causes an uncompensated spectral contribution.

y-cut quartz acting as the local oscillator (LO) and a $SrTiO_3$ plate for phase modulation. The SFG spectral interferogram created by the sample in reflection and the LO reflected from the sample was measured by a charge-coupled device–based polychromator. After this data acquisition, an SF intensity measurement of the sample with l_c^B configuration was performed in situ, where the condition of the MIR pulse was kept the same, but the NIR-A pulse was replaced by NIR-B with θ = 63.4 (±1)°. The SFG from the sample at another emission angle was detected with the same polychromator. The two spectra with l_c^A and l_c^B yielded the complex $\chi_{S,eff}^{(2),A}(\omega_2)$ and $\left|\chi_{S,eff}^{(2),B}(\omega_2)\right|^2$ of the sample, respectively, after normalization against a *z*-cut quartz crystal and correction of the Fresnel coefficients. Here, we adopted the slab model to calculate the interfacial dielectric function in the Fresnel factor correction (*29*, *30*, *49*). All measurements were performed with SSP-polarized SFG, NIR, and MIR fields at room temperature. We had λ = 1.3 μm, l_c^B = 70.6 nm, and l_c^A = 44.5 nm in water in all of the measurements except the wavelength-dependent test (Fig. 1, B and C) where l_c^B was varied in between 65.6 and 72.7 nm in water by tuning λ (= 1.18 to 1.37 μm).

Supplementary Materials

This PDF file includes:

Notes S1 and S2
Figs. S1 to S7
References

REFERENCES AND NOTES

1. L. Zhang, Y. Yang, Y.-T. Kao, L. Wang, D. Zhong, Protein hydration dynamics and molecular mechanism of coupled water-protein fluctuations. *J. Am. Chem. Soc.* **131**, 10677–10691 (2009).
2. N. Agmon, H. J. Bakker, R. K. Campen, R. H. Henchman, P. Pohl, S. Roke, M. Thamer, A. Hassanali, Protons and hydroxide ions in aqueous systems. *Chem. Rev.* **116**, 7642–7672 (2016).
3. P. P. Lopes, D. Strmcnik, J. S. Jirkovsky, J. G. Connell, V. Stamenkovic, N. Markovic, Double layer effects in electrocatalysis: The oxygen reduction reaction and ethanol oxidation reaction on Au(111), Pt(111) and Ir(111) in alkaline media containing Na and Li cations. *Catal. Today* **262**, 41–47 (2016).
4. H. Liu, B. E. Logan, Electricity generation using an air-cathode single chamber microbial fuel cell in the presence and absence of a proton exchange membrane. *Environ. Sci. Technol.* **38**, 4040–4046 (2004).
5. A. J. Bard, L. R. Faulkner, *Electrochemical Methods: Fundamentals and Applications* (Wiley, New York, 1980).
6. Y.-C. Wen, S. Zha, X. Liu, S. Yang, P. Guo, G. Shi, H. Fang, Y. R. Shen, C. S. Tian, Unveiling microscopic structures of charged water interfaces by surface-specific vibrational spectroscopy. *Phys. Rev. Lett.* **116**, 016101 (2016).
7. G. E. Brown, V. E. Henrich, W. H. Casey, D. L. Clark, C. Eggleston, A. Felmy, D. W. Goodman, M. Gratzel, G. Maciel, M. I. McCarthy, K. H. Nealson, D. A. Sverjensky, M. F. Toney, J. M. Zachara, Metal oxide surfaces and their interactions with aqueous solutions and microbial organisms. *Chem. Rev.* **99**, 77–174 (1999).
8. G. Gonella, E. H. G. Backus, Y. Nagata, D. J. Bonthuis, P. Loche, A. Schlaich, R. R. Netz, A. Kuhnle, I. T. McCrum, M. T. M. Koper, M. Wolf, B. Winter, G. Meijer, R. K. Campen, M. Bonn, Water at charged interfaces. *Nat. Rev. Chem.* **5**, 466–485 (2021).
9. R. Kusaka, S. Nihonyanagi, T. Tahara, The photochemical reaction of phenol becomes ultrafast at the air-water interface. *Nat. Chem.* **13**, 306–311 (2021).
10. C. Zhang, D. G. Knyazev, Y. A. Vereshaga, E. Ippoliti, T. H. Nguyen, P. Carloni, P. Pohl, Water at hydrophobic interfaces delays proton surface-to-bulk transfer and provides a pathway for lateral proton diffusion. *Proc. Natl. Acad. Sci. U.S.A.* **109**, 9744–9749 (2012).
11. J. Peng, J. Guo, P. Hapala, D. Cao, R. Ma, B. Cheng, L. Xu, M. Ondracek, P. Jelínek, E. Wang, Y. Jiang, Weakly perturbative imaging of interfacial water with submolecular resolution by atomic force microscopy. *Nat. Commun.* **9**, 122 (2018).
12. J.-J. Velasco-Velez, C. H. Wu, T. A. Pascal, L. F. Wan, J. Guo, D. Prendergast, M. Salmeron, The structure of interfacial water on gold electrodes studied by x-ray absorption spectroscopy. *Science* **346**, 831–834 (2014).
13. J. D. Smith, R. J. Saykally, P. L. Geissler, The effects of dissolved halide anions on hydrogen bonding in liquid water. *J. Am. Chem. Soc.* **129**, 13847–13856 (2007).
14. I. V. Stiopkin, C. Weeraman, P. A. Pieniazek, F. Y. Shalhout, J. L. Skinner, A. V. Benderskii, Hydrogen bonding at the water surface revealed by isotopic dilution spectroscopy. *Nature* **474**, 192–195 (2011).
15. S. Ong, X. Zhao, K. B. Eisenthal, Polarization of water molecules at a charged interface: Second harmonic studies of the silica/water interface. *Chem. Phys. Lett.* **191**, 327–335 (1992).
16. B. Rehl, J. M. Gibbs, Role of ions on the surface-bound water structure at the silica/water interface: Identifying the spectral signature of stability. *J. Phys. Chem. Lett.* **12**, 2854–2864 (2021).
17. P. E. Ohno, H.-f. Wang, F. M. Geiger, Second-order spectral lineshapes from charged interfaces. *Nat. Commun.* **8**, 1032 (2017).
18. J. Schaefer, E. H. G. Backus, M. Bonn, Evidence for auto-catalytic mineral dissolution from surface-specific vibrational spectroscopy. *Nat. Commun.* **9**, 3316 (2018).
19. S. Yang, M. Chen, Y. Su, J. Xu, X. Wu, C. Tian, Stabilization of hydroxide ions at the interface of a hydrophobic monolayer on water via reduced proton transfer. *Phys. Rev. Lett.* **125**, 156803 (2020).
20. A. Myalitsin, S.-h. Urashirna, S. Nihonyanagi, S. Yamaguchi, T. Tahara, Water structure at the buried silica/aqueous interface studied by heterodyne-detected vibrational sum-frequency generation. *J. Phys. Chem. C* **120**, 9357–9363 (2016).
21. S. H. Urashima, A. Myalitsin, S. Nihonyanagi, T. Tahara, The topmost water structure at a charged silica/aqueous interface revealed by heterodyne-detected vibrational sum frequency generation spectroscopy. *J. Phys. Chem. Lett.* **9**, 4109–4114 (2018).
22. N. G. Rey, E. Weißenborn, F. Schulze-Zachau, G. Gochev, B. Braunschweig, Quantifying double-layer potentials at liquid–gas interfaces from vibrational sum-frequency generation. *J. Phys. Chem. C* **123**, 1279–1286 (2019).
23. H. Wang, Q. Xu, Z. Liu, Y. Tang, G. Wei, Y. R. Shen, W.-T. Liu, Gate-controlled sum-frequency vibrational spectroscopy for probing charged oxide/water interfaces. *J. Phys. Chem. Lett.* **10**, 5943–5948 (2019).
24. L. Dalstein, E. Potapova, E. Tyrode, The elusive silica/water interface: Isolated silanols under water as revealed by vibrational sum frequency spectroscopy. *Phys. Chem. Chem. Phys.* **19**, 10343–10349 (2017).
25. E. H. G. Backus, D. Bonn, S. Cantin, S. Roke, M. Bonn, Laser-heating-induced displacement of surfactants on the water surface. *J. Phys. Chem. B* **116**, 2703–2712 (2012).
26. Y. He, Y. Shang, H. Liu, L. Dominique, S. Anniina, Surfactant adsorption onto interfaces: Measuring the surface excess in time. *Langmuir* **28**, 3146–3151 (2012).
27. I. Li, J. Bandara, M. J. Shultz, Time evolution studies of the H_2O/quartz interface using sum frequency generation, atomic force microscopy, and molecular dynamics. *Langmuir* **20**, 10474–10480 (2004).
28. C. Cai, M. S. Azam, D. K. Hore, Determining the surface potential of charged aqueous interfaces using nonlinear optical methods. *J. Phys. Chem. C* **125**, 25307–25315 (2021).

29. X. Wei, S. Hong, X. Zhuang, T. Goto, Y. R. Shen, Nonlinear optical studies of liquid crystal alignment on a rubbed polyvinyl alcohol surface. *Phys. Rev. E* **62**, 5160–5172 (2000).
30. X. Wei, thesis, University of California at Berkeley (2000).
31. T. Joutsuka, A. Morita, Electrolyte and temperature effects on third-order susceptibility in sum-frequency generation spectroscopy of aqueous salt solutions. *J. Phys. Chem. C* **122**, 11407–11413 (2018).
32. M. Peng, A. V. Nguyen, Adsorption of ionic surfactants at the air-water interface: The gap between theory and experiment. *Adv. Colloid Interface Sci.* **275**, 102052 (2020).
33. D. K. Hore, E. Tyrode, Probing charged aqueous interfaces near critical angles: Effect of varying coherence length. *J. Phys. Chem. C* **123**, 16911–16920 (2019).
34. E. Tyrode, R. Corkery, Charging of carboxylic acid monolayers with monovalent ions at low ionic strengths: Molecular insight revealed by vibrational sum frequency spectroscopy. *J. Phys. Chem. C* **122**, 28775–28786 (2018).
35. J. A. Mondal, S. Nihonyanagi, S. Yamaguchi, T. Tahara, Three distinct water structures at a zwitterionic lipid/water interface revealed by heterodyne-detected vibrational sum frequency generation. *J. Am. Chem. Soc.* **134**, 7842–7850 (2012).
36. L. B. Dreier, A. Wolde-Kidan, D. J. Bonthuis, R. R. Netz, E. H. G. Backus, M. Bonn, Unraveling the origin of the apparent charge of zwitterionic lipid layers. *J. Phys. Chem. Lett.* **10**, 6355–6359 (2019).
37. E. K. Perttu, A. G. Kohli, F. C. Szoka Jr., Inverse-phosphocholine lipids: A remix of a common phospholipid. *J. Am. Chem. Soc.* **134**, 4485–4488 (2012).
38. N. Ghosh, S. Roy, J. A. Mondal, Headgroup-specific interaction of biological lipid monolayer/water interface with perfluorinated persistent organic pollutant (f-POP): As observed with interface-selective vibrational spectroscopy. *J. Phys. Chem. B* **126**, 563–571 (2022).
39. T. Ishiyama, D. Terada, A. Morita, Hydrogen-bonding structure at zwitterionic lipid/water interface. *J. Phys. Chem. Lett.* **7**, 216–220 (2016).
40. S. Nihonyanagi, S. Yamaguchi, T. Tahara, Counterion effect on interfacial water at charged interfaces and its relevance to the Hofmeister series. *J. Am. Chem. Soc.* **136**, 6155–6158 (2014).
41. C. Dutta, M. Mammetkuliyev, A. V. Benderskii, Re-orientation of water molecules in response to surface charge at surfactant interfaces. *J. Chem. Phys.* **151**, 034703 (2019).
42. C. J. Moll, J. Versluis, H. J. Bakker, Direct evidence for a surface and bulk specific response in the sum-frequency generation spectrum of the water bend vibration. *Phys. Rev. Lett.* **127**, 116001 (2021).
43. Y. Nojima, S. Yamaguchi, Heterodyne-detected sum frequency generation spectroscopic study of weakly hydrogen-bonded water at charged lipid interfaces, revisited. *J. Phys. Chem. C* **125**, 23483–23489 (2021).
44. Y. Nojima, Y. Suzuki, S. Yamaguchi, Weakly hydrogen-bonded water inside charged lipid monolayer observed with heterodyne-detected vibrational sum frequency generation spectroscopy. *J. Phys. Chem. C* **121**, 2173–2180 (2017).
45. M. F. Bush, R. J. Saykally, E. R. Williams, Hydration of the calcium dication: Direct evidence for second shell formation from infrared spectroscopy. *ChemPhysChem* **8**, 2245–2253 (2007).
46. A. Patra, S. Roy, S. Saha, D. K. Palit, J. A. Mondal, Observation of extremely weakly interacting OH (~3600 cm^{-1}) in the vicinity of high charge density metal ions (M^{z+}; z = 1, 2, 3): A structural heterogeneity in the extended hydration shell. *J. Phys. Chem. C* **124**, 3028–3036 (2020).
47. S. Yuan, L. Ma, X. Zhang, L. Zheng, Molecular dynamics studies on monolayer of cetyltrimethylammonium bromide surfactant formed at the air/water interface. *Colloids Surf. A Physicochem. Eng. Asp.* **289**, 1–9 (2006).
48. L. Dalstein, K. Y. Chiang, Y.-C. Wen, Direct quantification of water surface charge by phase-sensitive second harmonic spectroscopy. *J. Phys. Chem. Lett.* **10**, 5200–5205 (2019).
49. X. Yu, K.-Y. Chiang, C.-C. Yu, M. Bonn, Y. Nagata, On the Fresnel factor correction of sum-frequency generation spectra of interfacial water. *J. Chem. Phys.* **158**, 044701 (2023).
50. X. Wei, Y. R. Shen, Motional effect in surface sum-frequency vibrational spectroscopy. *Phys. Rev. Lett.* **86**, 4799–4802 (2001).
51. A. Zdziennicka, K. Szymczyk, J. Krawczyk, B. Jańczuk, Activity and thermodynamic parameters of some surfactants adsorption at the water–air interface. *Fluid Ph. Equilibria* **318**, 25–33 (2012).

Acknowledgments: We thank the valuable discussions with H.-M. Lee and T.-M. Chuang. **Funding:** This work was funded by the National Science and Technology Council, Taiwan (grant numbers MOST 108-2112-M-001-039-MY3 and 111-2112-M-001-082-). **Author contributions:** Y.H. and Y.-C.W. designed the research project and performed the analyses. Y.H., T.-H.C., and A.P. conducted the experiments. Y.H., A.P., and Y.-C.W. discussed the results. T.-H.C. and Y.-C.W. wrote the manuscript. **Competing interests:** The authors declare that they have no competing interest. **Data and materials availability:** All data needed to evaluate the conclusions in the paper are present in the paper and/or the Supplementary Materials.

Submitted 13 December 2022
Accepted 14 March 2023
Published 12 April 2023
10.1126/sciadv.adg2823